Bakker A., Van den Akker H.E.A. (1994) A Computational Model for the Gas-Liquid Flow in Stirred Reactors. Chemical Engineering Research and Design, TransIChemE Vol. 72, Number A4, July 1994, page 573-582.

A COMPUTATIONAL MODEL FOR THE GAS-LIQUID FLOW IN STIRRED REACTORS

A. BAKKER and H. E. A. VAN DEN AKKER

Delft University of Technology, The Netherlands

In this paper a model is described for calculating the gas-liquid flow in stirred vessels. The general fluid flow code FLUENT is used for calculating the single-phase flow pattern. This flow pattern is used as input for an in-house code named GHOST! which calculates the distribution of the gas over the vessel on the basis of balance equations. A mathematical model for bubble break-up and bubble-coalescence, based on local turbulence intensity and local energy dissipation rate, is incorporated in this code. Details regarding modelling the impeller, bubble coalescence and bubble break-up are given in the paper. The GHOST! code is capable of calculating local void fraction, local bubble size, local interfacial area and local mass transfer. These local values can be integrated to yield the overall gas holdup and the overall mass transfer rate. There is a good agreement between computational results and measurements. Based on the simulations, it is concluded that full homogeneity of the gas-liquid mixture will never be achieved. This knowledge should be used in the optimization process.

Keywords: mixing; agitation; Computational Fluid Dynamics; gas-liquid flow; mass transfer; gas holdup

INTRODUCTION

Numerical computation of the flow field in stirred tank reactors has received attention since the beginning of the 1980s, starting with Harvey[1] and Harvey and Greaves[2,3]. Most times the computations are limited to single-phase flow although stirred vessels are widely used for multiphase mixing. Full computation of the flow field of a liquid phase in which a gas is dispersed has not been possible so far. This is partly due to a lack of knowledge of bubble dynamics and the influence of bubbles on the turbulence structure, and partly due to computational restrictions. In spite of the difficulties mentioned above, several attempts have been made to model the flow in a gassed stirred tank in a less rigorous way.

Issa and Gosman[4] calculated the flow in a gassed stirred vessel equipped with a disc turbine. In their calculations they assumed a very small (0.5 mm), constant bubble diameter. Further, they used very coarse grids and it was not possible to verify the results of their simulations because of a lack of experimental data.

Looney *et al.*[5] presented a model for the turbulent flow of solid/liquid suspensions in stirred vessels. This model incorporated mass balance and momentum balance equations, together with a two-phase turbulence model. Although the model predicted the mean velocities for both the phases reasonably well, the predictions of the turbulence intensities tended to separate from the experimental data. The predicted solids distributions could not be validated due to a lack of experimental data.

Pericleous and Patel[6] calculated both the single-phase flow and the two-phase flow in a stirred tank. Their calculations were done for various impeller types and combinations of impellers. Due to the use of a simple one-equation turbulence model (based on the Prandtl mixing-length hypothesis), their velocity predictions had a limited accuracy only. Their two-phase calculations were done assuming a constant bubble size and a constant bubble slip velocity, and the results could not be verified with experimental data.

From 1986 onwards, Mann[7,8] followed a different approach. He modelled the flow created by a disc turbine by a simple, two-dimensional network of zones, and calculated the gas transport in this network by solving the continuity equation for the gas phase. Although his results are interesting and have a qualitative appeal, the simplified model of the flow pattern and the local turbulence makes extension of the model to other geometries difficult.

An extensive model was proposed by Trägårdh[9]. He incorporated the momentum exchange between the gas phase and the liquid phase and models for local mass transfer and for the growth of microorganisms. However, his code was not capable of calculating the local bubble size and, like the other authors mentioned above, he did not take the influence of the turbulence on the bubble rise velocity into account.

Patterson[10] used the standard particle tracking model in FLUENT to calculate the gas distribution in a stirred vessel and performed LDA measurements on the gassed liquid velocities. His conclusions were that the liquid velocities near the tank wall increase on gassing, and that

0263-8762/94/$05.00 + 0.00
© Institution of Chemical Engineers

a significant amount of the input gas leaves the vessel near the baffles. The standard FLUENT model, however, leads to an over prediction of the overall gas holdup.

In a previous paper[11] it has been concluded that it is difficult to get insight in the processes occurring inside the gas-dispersion by measuring overall quantities. Since experimental measurements of the local gas holdup, bubble size, etc. are very tedious and not always possible, there is a strong need of models capable of calculating local gas holdup, local bubble size and local mass transfer rate.

In the current research project, the general fluid flow code FLUENT is used for calculating the single-phase flow in a stirred vessel equipped with either an axial flow impeller or a disc turbine[12]. This flow pattern, including the turbulence distribution, is used as input for an in-house code named GHOST! (Gas Holdup Simulation Tool!) that calculates the distribution of the gas over the vessel on the basis of balance equations assuming that the influence of the gas on the liquid flow is negligible, which will be the case when the gas holdup is sufficiently low. A mathematical model for bubble break-up and bubble coalescence, based on local turbulence intensity and local energy dissipation rate as calculated by FLUENT, is incorporated in this code. GHOST! is capable of calculating local values of void fraction, bubble size, interfacial area and mass transfer. The model presented in this paper is an improved version of the previous model presented by Bakker and Van den Akker[13].

First the various modelling steps will be described. Then the simulation results will be discussed and compared with experimental data.

THE COMPUTATIONAL MODEL

Single- Phase Flow Pattern Computation

The single phase flow pattern (liquid only) is calculated by solving the momentum equations and mass conservation equation with the aid of the general purpose code FLUENT. The Algebraic Stress Model[14,15] is used for calculating the turbulent Reynolds stresses. The computational procedures, grids, impeller boundary conditions etc. are all described by Bakker and Van den Akker[12].

However, the assumption that the gassed linear liquid velocities are equal to the ungassed velocities

$$\tilde{u}_{1,g} = \tilde{u}_{1,u} \tag{1}$$

will not be valid. It has repeatedly been reported[11] that both the impeller power consumption and the pumping capacity of an impeller decrease on gassing. Joshi *et al.*[16] proposed the following relation for this decrease in pumping capacity, assuming that the decrease in pumping capacity is proportional to the decrease in power consumption:

$$Fl_{1,g} = Fl_{1,u}\frac{Po_g}{Po_u} \tag{2}$$

Here Fl_u and Fl_g are the impeller pumping number in ungassed conditions and gassed conditions respectively. Po_u and Po_g are the ungassed and gassed power number. Thus, like Bakker and Van den Akker[13] the gassed liquid velocities were calculated with:

$$\tilde{u}_{1,g} = \tilde{u}_{1,u}\frac{Po_g}{Po_u} \tag{3}$$

The values for Po_u and Po_g used here are experimentally determined values according to the measurement procedures described by Bakker and Van den Akker[11]. Further, the turbulence properties need to be corrected for the effects of gassing. Two effects are important. First, the energy dissipation rate decreases due to the decrease in the impeller power consumption. Second, there will be an increase in the energy dissipation rate due to the power input of the gas. The k and ε values as calculated by FLUENT for the ungassed conditions (ε_u and k_u) will be corrected for both effects.

The energy input per second for a single bubble P_b is given by:

$$P_b = \vec{F}_s.\vec{u}_s \tag{4}$$

Here $\vec{F}_s$ and $\vec{u}_s$ are the slip force vector and the slip velocity vector respectively. Therefore the total energy dissipation rate under gassed conditions will be:

$$\varepsilon_g = \varepsilon_u\frac{Po_g}{Po_u} + \frac{n_b P_b}{\rho_l(1-\alpha)} \tag{5}$$

In the computation of the turbulent kinetic energy under gassed conditions, the Taylor macro scale of turbulence is used:

$$L_t = \frac{k^{3/2}}{\varepsilon} \tag{6}$$

It is assumed that the turbulent kinetic energy which results from the energy input by the impeller has the same Taylor length scale both under gassed and ungassed conditions, in other words: the turbulence structure which results from the energy input by the impeller is not affected by the gas. Further, it is likely that the energy input of the bubbles is dissipated through turbulent eddies containing the kinetic energy k_b and having a Taylor macro scale of the order of the bubble diameter:

$$d_b = k_b^{3/2}\left[\frac{n_b P_b}{\rho_l(1-\alpha)}\right]^{-1} \tag{7}$$

Now the following model equation for k under gassed conditions can be derived:

$$k_g = k_u\left(\frac{Po_g}{Po_u}\right)^{2/3} + \left[d_b\frac{n_b P_b}{\rho_l(1-\alpha)}\right]^{2/3} \tag{8}$$

Here d_b, α, ρ_l and n_b are the bubble diameter, the gas holdup, the liquid density and the bubble number density respectively. These model equations should be regarded as first order corrections and do not necessarily give a complete description of the physical mechanisms. For example, it is probable that the energy input by the gas bubbles will result in non-isotropic turbulence. However, the corrections for the influence of gassing on the mean velocities and the turbulence properties are small when the gas holdup is low, in which region the model predictions will be sufficiently accurate.

Transport Equations for the Gas-Phase

The single-phase flow pattern as calculated by FLUENT is used for calculating the transport of the gas throughout the vessel using the model equations given below.

The continuity equation for the gas-phase reads:

$$\frac{\partial \alpha}{\partial t} + \vec{\nabla}.(\alpha \vec{u}_g) = S_g \tag{9}$$

Here $\vec{u}_g$ denotes the linear gas velocity and S_g is the gas source. In a stirred vessel S_g is non-zero at the sparger only. On performing the Reynolds decomposition and averaging the equation we get for a steady-state situation:

$$\vec{\nabla}.(\bar{\alpha}\overline{\vec{u}_g}) + \vec{\nabla}.(\overline{\alpha'\vec{u}_g'}) = \overline{S_g} \tag{10}$$

The second term on the left-hand side describes the transport of gas due to the turbulent motion of the gas-phase and is not known in general. This leads to a so-called closure problem. This turbulent transport can be modelled on the analogy of the kinetic gas theory. Figure 1 shows the diffusional flux of randomly moving particles, as described by the kinetic gas theory[17]. In this figure n denotes the number density of the particles and $\bar{c}$ is the average of the fluctuating velocity of the particles. Further, λ_t denotes the so-called transport free path:

$$\lambda_t = C_\lambda \frac{1}{\sqrt{2}\pi d^2 n} \tag{11}$$

where C_λ is a model constant of the order unity. The net particle flux J_{net} duc to random motion from cell A to B is given by:

$$J_{net} = J_{AB} - J_{BA} = \tfrac{1}{4}(n\bar{c})_{-\lambda_t} - \tfrac{1}{4}(n\bar{c})_{\lambda_t} \tag{12}$$

GHOST! calculates the turbulent transport of the gas due to turbulent motion according to equation (12) where the average value of the particle velocity $\bar{c}$ equals the time average of the absolute value of the fluctuating component of the linear gas velocity:

$$\bar{c} = |\overline{\vec{u}_g'}| \tag{13}$$

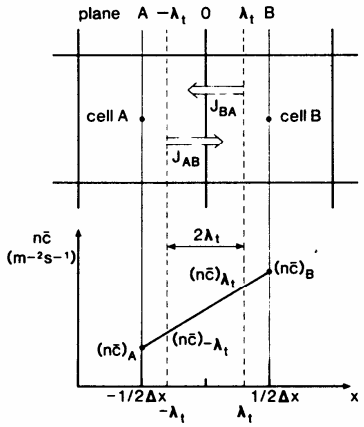

Figure 1. Flux of random moving particles from cell A to cell B and vice versa.

When the equations are written out further, this model can be reduced to a diffusion type of closure, and equation (10) becomes:

$$\vec{\nabla}\cdot(\bar{\alpha}\overline{\vec{u}_g}) - \vec{\nabla}(\mathbf{D}\bar{\alpha})) = \overline{S_g} \tag{14}$$

The turbulent diffusion coefficient $\mathbf{D}$ is given by:

$$\mathbf{D} = \tfrac{1}{3}\lambda_t|\overline{\vec{u}_g'}| \tag{15}$$

Note that the turbulent diffusion coefficient in equation (14) appears after the second $\vec{\nabla}$, thus reflecting the transport due to both gradients in mean gas holdup and due to gradients in the turbulence intensity. The latter effect has its analogy in the kinetic theory of gases in a phenomenon called thermo-diffusion: diffusion due to gradients in temperature.

Further, we assume that the average random fluctuating velocity of the gas phase is proportional to that of the liquid phase:

$$|\overline{\vec{u}_g'}| \sim |\overline{\vec{u}_l'}| \approx \sqrt{2k} \tag{16}$$

the linear gas velocity is calculated as the sum of the linear liquid velocity and the slip velocity between the two phases:

$$\vec{u}_g = \vec{u}_{l,g} + \vec{u}_s \tag{17}$$

Here $\vec{u}_{l,g}$ denotes the linear liquid velocity under gassed conditions. The computation of $\vec{u}_{l,g}$ was discussed in section 2.1. The slip velocity $\vec{u}_s$ can be calculated by a force balance on the bubbles (in (r, ϕ, z) coordinates):

$$-\rho_l V_b \frac{w^2}{r}\hat{r} - \rho_l g V_b \hat{z} = C_D \tfrac{1}{2}\rho_l |\vec{u}_s|\vec{u}_s \frac{\pi}{4} d_b^2 \tag{18}$$

Here V_b denotes the bubble volume, $\hat{r}$ is the unity vector in the radial direction and $\hat{z}$ is the unity vector in the axial direction. The force in the radial direction equals the centripetal force on the bubbles, while the force in the vertical direction is of course the buoyancy. The bubbles follow the main liquid flow in the circumferential direction.

The constant C_D is a function of the bubble Reynolds number and can be calculated from the correlations given by Morsi and Alexander[18]. Their correlations are strictly speaking only valid for particles moving in a stagnant liquid. To account for the influence of turbulence in our case, we calculate the bubble Reynolds number with a modified viscosity term. This method was inspired by the work of Barnea and Mizrahi[19], although these authors used the modified viscosity approach to correct for mutual hindrance effects in bubble clouds instead of for the influence of turbulence. The modified bubble Reynolds number is now given by:

$$Re_b = \frac{\rho_l |\vec{u}_s| d_b}{\eta_*} \tag{19}$$

Here η_* is the sum of the liquid viscosity and a term proportional to the turbulent viscosity:

$$\eta_* = \eta_l + C_* \rho_l \frac{k^2}{\varepsilon} \tag{20}$$

This extra term, incorporating the model constant C_*, is introduced to account for the decrease in slip velocity

when a bubble is moving in a turbulent flow field instead of in a stagnant liquid. This decrease in slip velocity is due to the increased momentum transport around the bubble, and will be dependent on the ratio between the bubble size and the turbulent length scale. Thus C_* will be zero for bubbles smaller than the Kolmogorov length scale and will increase with bubble size. However, to prevent unnecessary complications the computations presented in this paper were performed with a constant value of C_*. Since not all turbulent eddies of all length scales will affect the momentum transport around the bubble, C_* will be smaller than the constant C_μ in the k-ε model described by Bakker and Van den Akker[12].

Bubble Formation

The number of bubbles per dispersion volume n_b is related to the gas holdup and the average bubble volume in the volume element investigated:

$$n_b = \frac{\alpha}{V_b} \tag{21}$$

The conservation equation for the bubble number density n_b reads:

$$\frac{\partial n_b}{\partial t} + \vec{\nabla}.(n_b \vec{u}_g) = \dot{n}_{b,c/b} + \frac{S_g}{V_{b,in}} \tag{22}$$

Here $\dot{n}_{b,c/b}$ denotes the change in n_b due to coalescence and breakup. An estimation for $\dot{n}_{b,c/b}$ can be made by performing some bubble cloud statistics. Think of a closed volume filled with a turbulent coalescing liquid containing a certain number of very small bubbles n_{b0}. Due to coalescence and breakup, the number of bubbles will gradually decrease, and the average bubble size will increase, until an equilibrium is reached at $n_{b\infty}$, see also Figure 2. Such a process could be modelled assuming an exponential decrease in the number of bubbles:

$$\frac{\partial n_b}{\partial t} = \omega(n_{b\infty} - n_b) \tag{23}$$

In this equation ω denotes an average effective coalescence/breakup frequency. It is likely that this coalescence dominated process results in an average bubble size proportional to the maximum stable bubble size according to Hinze[20].

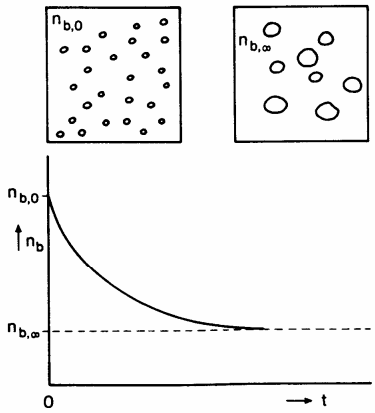

Figure 2. Decrease in bubble number density in case the bubble formation process is coalescence dominated.

$$d_{b\infty} = C_{b\infty}\left(12\,\frac{\sigma}{\rho_l}\right)^{3/5} \varepsilon^{-2/5} \tag{24}$$

A model constant $C_{b\infty}$ has been added in this equation. The bubble size in the outflow of the impeller is directly calculated with equation (24), on basis of the average energy dissipation rate inside the impeller. Therefore $C_{b\infty}$ is estimated to be 0.4 from bubble size data reported by Greaves and Barigou[21]. Since the energy dissipation rate in the outflow of the impeller decreases faster than the bubble size can increase, the maximum stable bubble size in the bulk of the stirred vessel is larger than the average bubble size.

As a result the bubble formation process in the bulk is coalescence dominated. In this case the decrease in bubble number density is given by:

$$\frac{\partial n_b}{\partial t} = -X_c f \tag{25}$$

Here f is the total number of bubble collisions, which can be calculated according to an analogy with the kinetic theory of gases:

$$f = \frac{3}{2}\sqrt{2}\,\frac{\alpha}{d_b}\,|\overline{u_g'}|n_b \tag{26}$$

Further, X_c denotes the efficiency of the process. Only part of the collisions leads to coalescence. With increasing bubble size there is an increasing chance that newly formed bubbles will break again because they have become too large. Thus X_c will decrease when the ratio $n_{b\infty}/n_b$ increases. A first order approximation for X_c can be made:

$$X_c = C_\omega\left(1 - \frac{n_{b\infty}}{n_b}\right) \tag{27}$$

In this equation C_ω is a model constant the value of which depends, amongst other things, on the properties of the medium. The equations above can be combined to give the new conservation equation for n_b:

$$\frac{\partial n_b}{\partial t} + \vec{\nabla}.(n_b \vec{u}_g) = \omega(n_{b\infty} - n_b) + \frac{S_g}{V_{b,in}} \tag{28}$$

in which the average effective coalescence/breakup frequency is given by:

$$\omega = C_\omega \frac{3}{2}\sqrt{2}\,\frac{\alpha}{d_b}\,|\overline{\vec{u}_g'}| \tag{29}$$

Equations (28) to (29) are used for calculating the local bubble size in the bulk of the dispersion volume. The equations given above can also be combined to yield the equation for conservation of bubble volume:

$$\frac{\partial V_b}{\partial t} + \vec{u}_g.\vec{\nabla}V_b = \omega V_b\left(1 - \frac{V_b}{V_{b\infty}}\right) + \frac{1}{\alpha}S_g V_b\left(1 - \frac{V_b}{V_{b,in}}\right) \tag{30}$$

Mass Transfer

When the local gas holdup and local bubble size are known, the mass transfer coefficient $k_l a$ can be calculated by using the equation for k_l given by Kawase and Moo-Young[22].

$$k_l = 0.301(\varepsilon\nu)^{1/4} Sc^{-1/2} \tag{31}$$

Sc is the Schmidt number. In the model equations given above it is assumed that the bubbles are spherical. It is, however, more likely that the bubbles are ellipsoidal and have a larger surface area than spherical bubbles. To check whether this suspicion is justified, the correlation of Wellek *et al.*[23] for the ratio a/b between the long and short axis of an ellipsoidal bubble has been used:

$$\frac{a}{b} = 1 + 0.163 Eo^{0.757} \left(Eo < 40; \frac{g\mu^4 \Delta\rho}{\rho^2 \sigma^3} \leq 1.10^{-6} \right) \tag{32}$$

Here Eo denotes the Eötvös number, which is defined by:

$$Eo = \frac{\Delta\rho g d_b^2}{\sigma} \tag{33}$$

The volume of an ellipsoidal bubble is given by:

$$V_b = \tfrac{4}{3}\pi a^2 b \tag{34}$$

The surface area of an ellipsoidal bubble can be calculated from:

$$A_b = 2\pi a^2 \left(1 + \frac{b}{a} \frac{\ln\left(\frac{a}{b} + \sqrt{\frac{a^2}{b^2} - 1} \right)}{\sqrt{\frac{a^2}{b^2} - 1}} \right) \left(0 < \frac{b}{a} < 1 \right) \tag{35}$$

Finally the local mass transfer coefficient per dispersion volume can be calculated from:

$$k_l a_d = k_l n_b A_b \tag{36}$$

and the local mass transfer coefficient per liquid volume is given by:

$$k_l a = k_l a_d \frac{1}{1 - \alpha} \tag{37}$$

GHOST! reports the values for $k_l a$ and $k_l a_d$ as calculated assuming spherical bubbles, and as calculated assuming ellipisoidal bubbles. Since the ratio a/b is in general smaller than 1.3, the difference between the two methods was smaller than 1%.

The GHOST! Code

On basis of the equations above GHOST! (Gas Holdup Simulation Tool!) has been developed. GHOST! is a finite difference code, written in PASCAL, which is capable of calculating local values of void fraction, bubble size, interfacial area and mass transfer.

GHOST! starts with reading in the velocity-file. This is a FLUENT lineprint file converted to GHOST! format. This file contains the coordinates the the grid nodes, the mean velocities, k and ε.

The GHOST!-case file contains, amongst other things, the values of the model constants, the position of the sparger, the gas input, Po_u, Po_g, the properties of the liquid medium and the solution parameters. Important solution parameters are the convergence criterion, the maximum number of iterations and the under relaxation parameters.

The user can provide GHOST! with an initial guess for α and d_b assuming homogeneous distributions, or a gas-file containing data from a previous calculation can be used. After the cell properties are calculated, the mean velocities and the k and ε values are corrected according to Po_g/Po_u. In the main loop the important quantities are updated sequentially until the solution is converged. The convergence criterion used was that the relative change in α and d_b in successive iterations was smaller than 0.001 in each computational cell, and that the difference between the amount of gas escaping at the liquid surface and the amount of gas issuing from the sparger was also smaller than 0.1%.

GHOST! generates two output files after the solution is converged. The gas-file contains the local values of α, d_b, $k_l a$ and $\tilde{u}_s$. This file can be used as input file to provide GHOST! with an initial guess for further calculations but can also be converted to FLUENT format for graphics processing. The log-file contains the case file and a general list of results, as there are: the average values and maxima and minima of α, d_b, $k_l a$, $d_b/d_{b\infty}$ and $\tilde{u}_s$. Examples of other listed variables are: the rate of convergence, the values of several important quantities integrated over the impeller zone and the bubble size near the liquid surface.

The calculations can be performed on any type of 2D or 3D, uniform or non-uniform, cylindrical finite-difference grid. The staggered grid convention is used, which means that all the velocities are stored on the cell faces whereas the other properties are stored on the node centers. A first order upwind differencing scheme is employed for interpolation to the cell faces.

The computational algorithms are set up in a very flexible way and are not limited to any particular geometry, which means that a quick assessment of the influence of geometrical changes, for example sparger position and impeller placement, on gas holdup and mass transfer can be made.

EXPERIMENTAL

For the purpose of validation of the calculated gas holdup profiles, local gas holdup measurements were performed using a single-point optical fibre probe. The overall holdup was determined with the aid of an ultrasonic liquid level meter. The overall mass transfer coefficient $k_l a$ (per liquid volume) was measured with a dynamic method Bakker[24].

For measuring the bubble size an optical four point probe has been used. This measurement method was developed by Frijlink[25], see also Bakker[24]. However, due to the dimensions of this probe, bubbles smaller than 1.4 mm can not be measured. Further, it is necessary that the probe is positioned in the direction of the main

Table 1. Geometrical details. The values of $Fl_{i,u}$ are experimental values. The values of $Fl_{i,g}$ are calculated according to equation (2).

			N(Hz)	V_{sg}(m/s)	P/V_l	Po_u	Po_g	Fl_g	$Fl_{i,u}$	$Fl_{i,g}$
1	DT	(LRS)	5.55	0.0036	1520	5.10	3.59	0.019	0.76	0.55
2	A315	(LRS)	10.0	0.0036	1520	0.76	0.58	0.010	0.74	0.56
3	A315	(SRS)	9.95	0.0036	1520	0.76	0.59	0.010	0.74	0.57
4	PBT	(LRS)	8.00	0.0036	1520	1.55	1.19	0.013	0.81	0.62
5	PBT	(LRS)	8.00	0.0007	1950	1.55	1.52	0.002	0.81	0.79

bubble flow. Due to these restrictions, the bubble size could only be measured near the liquid surface. In this region the bubbles are large enough to be measured with the four point probe and the probe can easily be positioned along the direction of the main bubble flow.

All the experiments were done in a perspex vessel of 0.444 m diameter. Impellers tested were a pitched blade impeller (PBT) with six blades, at 45° blade angle, a Lightnin A315 impeller, and a disc turbine (DT). Two sparger configurations were used, a large ringsparger (LRS, $d_s/D = 0.75$) mounted at a distance $S = 0.6\ D$ from the impeller and a small ringsparger (SRS, $d = 0.4\ D$) mounted at $S = 0.2\ D$ from the impeller. The impellers were mounted at a distance $C = 0.75\ D$ from the bottom. The impeller diameter was $D = 0.4\ T$ in all cases. The experimental details are listed in Table 2. Both the A315 and the PBT were operated in the indirect loading regime. The PBT was tested at two different gassing rates.

RESULTS

Overall Quantities

Several sets of model parameters were tested. The parameter set which gave the best results is listed in Table 2. It should be noted that Bakker and Van den Akker[13] used $C_\omega = 0.2$ instead of $C_\omega = 0.15$ and $C_{b\infty} = 0.75$ instead of $C_{b\infty} = 0.4$. However, this led to under predicting the mass transfer coefficient k_la, which is not the case with the present parameter set. The simulations and the experimental data were found to match quite well, (see Table 3). Both the overall gas holdup and the overall mass transfer coefficient k_la are predicted quite accurately, especially with the disc turbine and the PBT. With the A315 the predicted overall holdup is somewhat smaller than the measured holdup.

Table 2. The model parameters used in the simulations.

C_ϵ	$C_{b\infty}$	C_ω	C_λ
0.02	0.4	0.15	1.0

Table 3. Overall experimental and simulation results. The cases are numbered in the same order as in Table 1.

		α(%) Exp	α(%) Sim	$\langle d_{b,out}\rangle$ Exp	(mm) Sim	k_l(1/s) Exp	k_la(1/s) Sim
1	DT	4.7 ± 0.2	4.9	3.25	2.91	0.038	0.038
2	A315	4.6 ± 0.2	4.2	3.76	3.59	0.035	0.036
3	A315	4.8 ± 0.2	4.3	—	3.82	0.038	0.036
4	PBT	4.1 ± 0.3	4.1	3.44	3.39	0.036	0.037
5	PBT	1.1 ± 0.3	1.0	—	2.00	0.011	0.013

With the A315 the influence of sparger position was tested. Both experimental results and model calculations show that the overall gas holdup increases when the sparger is made smaller and mounted closer to the impeller. The experimental data show that the overall mass transfer coefficient also increases. This effect was already reported by Bakker and Van den Akker[26] and by Bakker and Van den Akker[11]. The model predictions, however, do not show this increase in k_la due to the fact that the increase in gas holdup leads to increased coalescence rates and thus to larger bubbles. This can be seen from the computed average size of the bubbles which leave the vessel. As a consequence the interfacial area does not increase with increasing holdup in this case. This might mean that the coalescence rate model presented here shows a slightly too strong dependence on local holdup, but direct experimental verification is virtually impossible.

Note that although the gas holdup predicted with the disc turbine is quite high relative to the other two impellers, the difference in k_la between the impellers is smaller. This is due to the fact that with the *DT* most of the turbulent kinetic energy is dissipated in the relatively small volume around the impeller. A significant part of the gas in the vessel is thus found in regions with a low turbulence intensity and with low k_l values. Part of the differences between the experimental data and the predicted data can be accounted for through experimental inaccuracies. In Table 3 the standard deviation in the measurements of the overall gas holdup is also listed. It is inevitable that the experimental data for the bubble diameter and the k_la also contain inaccuracies. However, the accuracy of these methods was difficult to estimate.

Further, certain assmptions in the model described above may also account for deviations between the model predictions and the experimental data. This will be discussed in more detail in Section 5.

Local Gas Holdup

For verification of the modelling results, measurements of the local gas holdup have been performed at various positions inside the vessel. Figure 3a shows a comparison between the predicted local gas holdup and the experimentally determined values for the disc turbine. It can be seen that peaks in the gas holdup are found right above the sparger and in the lower circulation loop, near the vessel wall where gas and liquid are in counterflow. In general, the predicted holdup profiles match the experimental data quite well, except in the upper part of the vessel near the shaft. According to the model predictions, the holdup decreases in this region, something which is not confirmed by the experimental

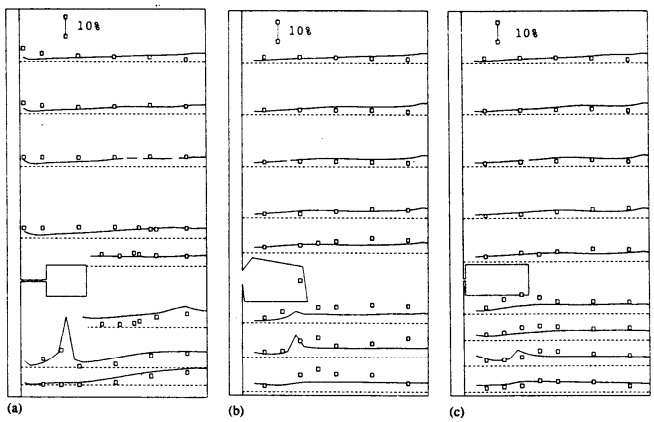

Figure 3. Comparison between predicted and measured gas holdup profiles for the disc-turbine, the A315 and the pitched blade turbine respectively. (□ experimental, ——— simulation, $\phi = 45°$, $P/V_l = 1520\ \mathrm{Wm^{-3}}$, $v_{sg} = 0.0036$ m/s)

data. This might be due to an under predicted gas recirculation rate or a too short recirculation loop.

The results for the A315 and the PBT are shown in Figures 3b and 3c. As with the DT, peaks in the gas holdup are found near the sparger, and in the lower part of the vessel. Several regions can be distinguished. The predicted holdup profiles and the experimentally measured values match quite well in the lower part of the vessel near the wall. Good agreement is also achieved in the region directly above the impeller. Near the liquid surface the experimental and simulated profiles tend to separate. Visual observation of the vessel revealed that in this part of the vessel the bubbles rise relatively undisturbed through the centre as if it were a bubble column, and sometimes moves downwards near the vessel wall. This might mean that in this region the gas-flow is strong relative to the liquid flow and induces a secondary circulation loop.

Further, due to the fact that these axial flow impellers disperse the gas from strong trailing vortices (see Figures 3b and 3c, below the impeller blade tip), peaks in the gas holdup are measured in the region which stretches from the impeller blade tip to the vessel bottom. Since no quantitative impeller model which predicts such vortices is available, these peaks could not be predicted. This leads to differences between the experimental data and the predicted profiles in this region.

Figure 4 shows the local gas holdup in the plane just above the pitched blade turbine ($z/H = 0.66$). From this graph it can be seen that the gas distribution is three dimensional. At small radial distances the gas distribution is approximately axisymmetric, but this is not the case near the baffles.

Local Bubble Size

Figure 5a,b,c show the computed contours of local bubble size for the disc-turbine, for the A315 and for the pitched blade turbine in the plane midway between the baffles.

From these figures it can be seen that for all three impellers the spatial bubble size distribution is clearly non-homogeneous. For all impellers the smallest bubbles are found in the outflow of the impellers. The bubble size increases along the circulation loops, due to coalescence. The interaction between local gas holdup, local bubble size and the local turbulence intensity is quite complex. A high gas holdup leads to large coalescence rates because of the large number of bubble collisions. A high turbulence intensity, especially the kinetic energy contained in the eddies of a wave-length of the order of the bubble diameter, will lead to an increase in bubble break-up, but also to increased coalescence as a result of the increase in the bubble collision rate. It will depend on the bubble size, the maximum stable bubble size, the gas holdup and the turbulence intensity which of the two mechanisms dominates.

A small bubble size leads to reduced slip velocities, which leads to an increase in gas holdup, which as explained above leads again to an increase in bubble size.

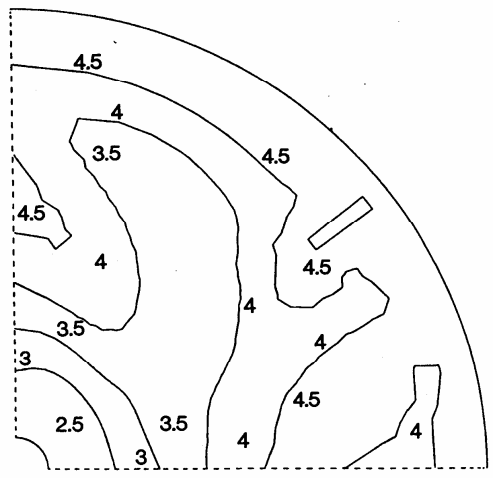

Figure 4. Contours of constant gas holdup (%) for the pitched blade turbine, top view, GHOST!-simulation. The numbers denote the minimum values in the areas enclosed by the contours, $z/H = 0.66$ (just above the impeller), $1520\ \mathrm{Wm^{-3}}$, $v_{sg} = 0.0036$ m/s.

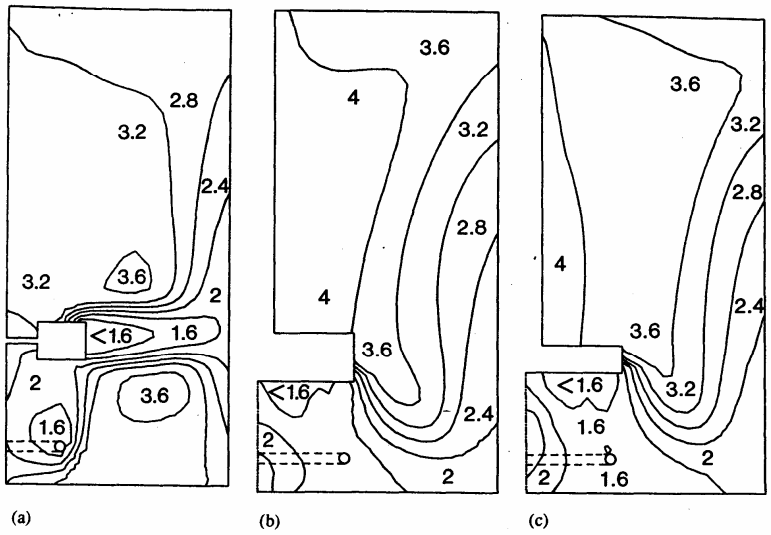

Figure 5. Contours of constant bubble size (mm) for the disc-turbine, the A315 and the pitched blade turbine. The numbers denote the minimum values in the areas enclosed by the contours. ($\phi = 45°$, $P/V_l = 1520\ \mathrm{Wm^{-3}}$, $v_{sg} = 0.0036$ m/s)

Further, the impeller breaks up the gas bubbles and acts as a source of small bubbles. Thus there are several mechanisms interacting, some of them mutually counteracting. The final spatial bubble size distribution is a complex function of the convective bubble transport, bubble break-up by the impeller and the local turbulence intensity.

In Figures 6, 7 and 8 the predicted bubble size and the experimentally determined bubble size are plotted as a function of the radial distance $2r/D$ at $\phi = 45°$ and at $z/H = 0.045$ ($P/V_l = 1520\ \mathrm{Wm^{-3}}$, $V_{sg} = 0.0036\ \mathrm{ms^{-1}}$). All experimental data points are averages of 200 bubbles. It can be seen that GHOST! predicts for all three impellers that the bubble size increases slightly towards the shaft, as a result of coalescence. With the PBT and the A315 an increase in gas holdup is found near the shaft, where the liquid flow is directed downwards. This also leads to an increase in bubble size. The scatter in the experimental data points is too large to confirm this

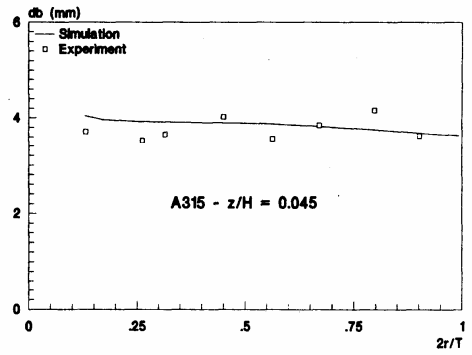

Figure 7. Comparison between predicted and measured bubble size, A315.

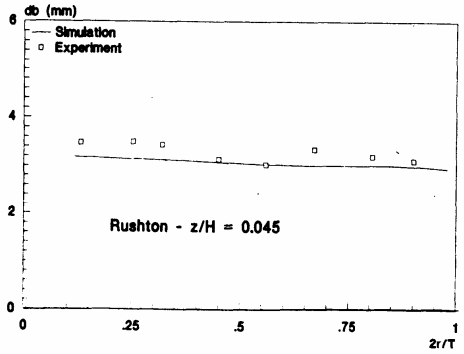

Figure 6. Comparison between predicted and measured bubble size, disc-turbine.

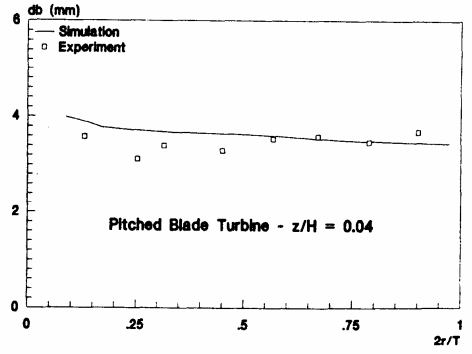

Figure 8. Comparison between predicted and measured bubble size, pitched blade turbine.

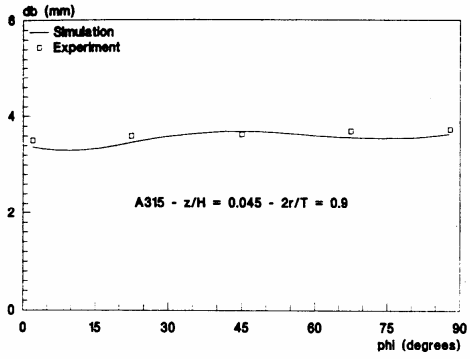

Figure 9. Comparison between predicted and measured bubble size, A315.

although in general there is a good agreement between the predicted bubble size and the experimental data.

Figure 9 shows a comparison between the experimental and predicted values of the bubble size near the vessel wall and near the liquid surface as a function of the circumferential coordinate ϕ. The simulations predict small three dimensional effects, with a local maximum in the bubble size at $\phi = 45°$ (midway baffles). However, the number of experimental data points is too limited for a detailed verification.

Figure 10 shows a measured bubble size distribution for the PBT. It can be seen that the bubble size distribution is fairly wide, with a standard deviation of 0.9 mm at an average bubble size of 3.3 mm.

Note that both the model predictions and the experimental data (see also Table 3) show that there are significant differences in the size of the bubbles which leave the vessesl. With the DT the bubble size is a bit smaller than with the axial flow impellers, due to the fact that with this impeller the gas bubbles first enter the impeller, which breaks them up, before they are distributed through the vessel. Further, the bubble path from the disc turbine to the liquid surface is shorter than from the sparger below an axial flow impeller to the liquid surface. Thus the bubbles have less time to coalesce before they leave the vessel.

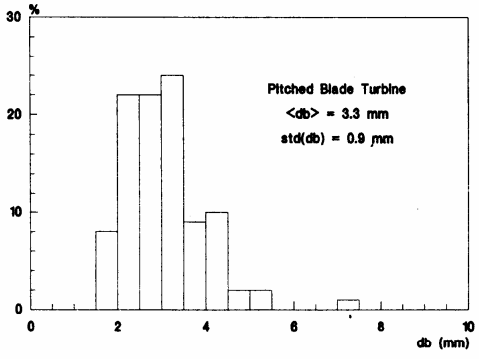

Figure 10. Typical experimental bubble size distribution, PBT, $\phi = 45°$, $2r/T = 0.9$, $z/H = 0.045$

The pitched blade turbine creates somewhat smaller bubbles than the A315. This might either be due to the lower gas holdup or to differences in the turbulence distribution, or both.

The fact that experimental and predicted values for $\langle d_{b,out} \rangle$ in Table 3 do not quite match is partly due to the fact that these averages are computed in a different way. The experimental values are calculated as

$$\langle d_{b,out} \rangle = \frac{1}{N} \sum_{i=1}^{N} d_{b,i} \tag{39}$$

for all measured bubbles at $z/H = 0.045$ and $\phi = 45°$. The predicted values are calculated as:

$$\langle d_{b,out} \rangle = \left[\frac{-1}{N_{b,out}} \int_0^{2\pi} \int_0^{R} (\hat{z}.\vec{u}_g)\alpha \frac{1}{V_b} d_b r \, dr \, d\phi \right]_{z=0} \tag{40}$$

Here $N_{b,out}$ denotes the total number of bubbles leaving the vessel per second. This surface integral gives the average diameter of all bubbles leaving the vessel.

Local Mass Transfer Rate

Figures 11a,b,c show contours of constant $k_l a$ for the disc turbine, the A315 and the pitched blade turbine. The local mass transfer rate $k_l a$ is determined by both the local values of the interfacial area a and the mass transfer coefficient k_l. The local value of the interfacial area follows from the local gas holdup and the local bubble size, which are each described in the previous sections. The mass transfer coefficient k_l does not so much depend on the bubble properties. Since the main resistance for mass transfer is on the liquid side it is mainly the local turbulence intensity which determines k_l. Thus k_l will be high in regions with a high turbulence intensity, since the turbulence intensity determines the process of surface renewal in the stagnant liquid film around the bubble.

It can be seen from Figure 11a,b,c that the highest $k_l a$ values are found in the outflow of the impeller. Very low $k_l a$ values are found in the liquid bulk. For the disc turbine about 31% of the mass transfer takes place in just 7.8% of the liquid volume. For the PBT these figures are 14% of the $k_l a$ in 4.8% of the liquid volume. With the A315 12% of the mass transfer takes place in the impeller and the outflow of the impeller, this being only 5% of the total volume.

DISCUSSION

Model Validity

A model has been presented with which local values of the gas holdup, bubble size, k_l, a and $k_l a$ can be calculated. The model predictions show an encouraging agreement with the experimental data. Depending on operating conditions the differences between the model predictions and the experimental results vary from 0% to $\pm 20\%$. This means that the model can be used as a research tool, and when the results are interpreted with care also as a design tool.

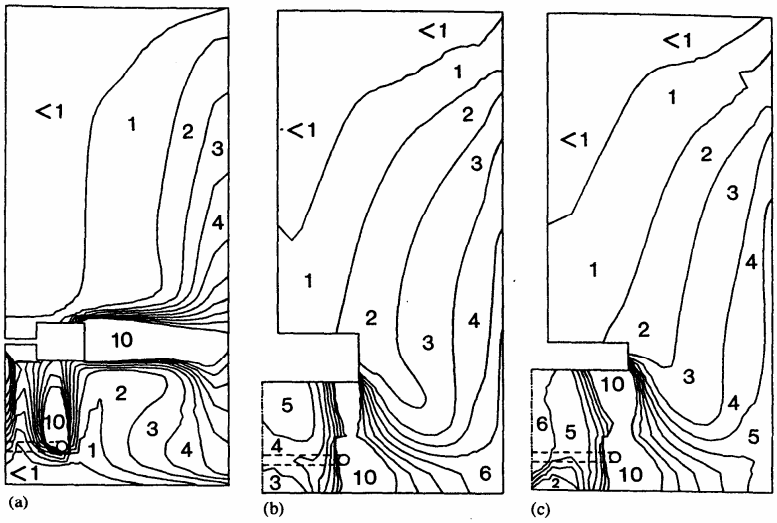

Figure 11. Contours of constant $100*k_l a$ (s^{-1}) for the disc-turbine, the A315 and the pitched blade turbine. The numbers denote the minimum values in the areas enclosed by the contours. ($\phi = 45°$, $P/V_l = 1520\ Wm^{-3}$, $v_{sg} = 0.0036$ m/s)

The gassed stirred vessel is, however, a notoriously complex system. Many phenomena like bubble formation, turbulence, impeller pumping capacity, vortex shedding, etc. have not been investigated in full detail. As a consequence, the model presented in this paper had to be based on a number of assumptions. The most important assumption is that the influence of the gas on the liquid flow is small, and can be described with a decrease in pumping capacity of the impeller, the decrease being proportional to the decrease in power consumption of the impeller on gassing. As a result, the model can only be applied with confidence at low gas flows. At higher gas flows both the momentum exchange between the gas flow and the liquid flow and a more advanced impeller model should be incorporated. The best way to model the impeller might be with the aid of experimental correlations for the impeller pumping capacity as a function of the impeller speed and the gas flow through the impeller. If such data were available, this would make the prediction of hydrodynamic transitions, such as the loading-flooding transition possible.

Another modelling problem is the way the gas is dispersed by the impeller. The experimental holdup data for the PBT and the A315 show that a significant amount of gas is dispersed from the trailing vortices, shed from the impeller blades. Unfortunately, the direct computation of the flow in trailing vortices is a far from trivial process, even in single-phase flow. As a consequence, models for the dispersion from such vortices will have to rely heavily on experimental data.

Further, in all the calculations steady-state flow is assumed. Bakker and Van den Akker[26] and Bakker and Van den Akker[11], reported that at certain gassing rates with axial flow impellers transient flow patterns can occur. It will be clear that predicting the transient behaviour of bubble clouds in agitated tanks is still far away.

The model incorporates four model constants. The values of these constants have been chosen by comparing the simulation results for various parameter sets with the available experimental data. The number of data, however, is limited. To improve the accuracy of estimating the model constants, more experimental data for a wide range of situations should be made available.

It can be concluded that the model described in this paper is applicable, provided that the gas flow is low, as a tool to gain insight in the physical processes in the gas dispersion. For the prediction of hydrodynamic transitions and the flow at high gassing rates, the model should be extended to a full two-phase model. Especially the quantitative modelling of the impeller remains a problem.

Interpretation of the Results

The main conclusion which can be drawn from the results from the simulations discussed above is that the spatial gas distribution is far from homogeneous for all impellers investigated. Although at a first glance this might seem a problem, that is not necessarily the case since the turbulence distribution generated by the impellers is also inhomogeneous. Since it is the local turbulence intensity at small turbulent length scales which determines the value of the mass transfer coefficient k_l it is advantageous to concentrate the gas in regions with a high turbulence intensity. In fact, this is why the disc turbine is capable of creating a mass transfer rate as high as that of the axial flow impellers, despite the relatively weak liquid flow, since with this impeller all the gas enters the impeller before it is dispersed.

It is impossible to create a really homogeneous gas dispersion in a stirred vessel. There will always exist regions where gas and liquid are in countercurrent flow and regions where both phases are in cocurrent flow.

This fact, in combination with pressure differences and centripetal forces, inevitably leads to spatial variations in the local gas holdup.

A similar argument can be applied to the turbulence distribution. The turbulence levels in the impeller region will always be higher than in the liquid bulk due to blade friction and vortex formation, even though carefully designed profiled blades can increase the energetic efficiency of the impeller.

The overall mass transfer rate follows directly from the spatial distribution of k_la. Since the k_la distribution is directly linked to the local α, d_b and ε values, optimization of the mass transfer performance will have to concentrate on matching the positions of the extremes in these spatial distributions. Given the fact that the gas distribution will always be non-homogeneous, the turbulence distribution should also be non-homogeneous, and vice-versa.

This does, however, not imply that one should aim at creating non-homogeneous gas and turbulence distributions. As a guideline one should aim at creating a mixture which is as homogeneous as possible, making use of the knowledge that full homogeneity will never be achieved in the optimization process.

It is not useful to design a system which is optimized with respect to one of the variables mentioned above. For example, a homogeneous turbulence distribution may well be disadvantageous when the α and d_b distributions are not adjusted accordingly. This is a difficult task, since the interaction between α, d_b and ε is very complex. Computer simulation is probably the only practical solution to this problem.

Matching the positions of extremes in the spatial distributions happens, to some extent, automatically with the disc turbine, since with this impeller the input gas will always be dispersed by the impeller before leaving the vessel. With axial flow impellers this is not necessarily the case, and the mass transfer performance can be improved by adjusting the positions of the impeller and the sparger. The use of special sparger types, which generate small bubbles at the gas inlet should also be considered, especially with axial flow impellers. It will be clear that the improvements in mass transfer rate which can be expected are larger with non-coalescing liquids, since then an increase in turbulence intensity will not necessarily lead to an increase in coalescence rates and bubble size.

In general it can be concluded that there is room for further optimization of stirred vessels with respect to mass transfer. There is no physical reason why the overall mass transfer rate should only depend on the overall power consumption and the overall gas input. However, there are several opposing mechanisms which dampen out the effects of large changes in the flow structure on the overall mass transfer rate, especially in coalescing systems like water. Examples are the decrease in impeller pumping capacity at a high pressure loading, and increased coalescence at high turbulence intensities and small bubble sizes. As a result the differences in k_la which can be expected in coalescing systems like air-water, are small and generally not larger than $\pm 10\%$ around the average. Since these improvements are of the same order as the inaccuracies in the present k_la measurement methods and computer simulations, more fundamental research remains necessary.

CONCLUSIONS

A model has been presented with which local values of holdup, bubble size and mass transfer can be calculated in a stirred vessel. All the model equations are incorporated in an in-house code named GHOST!, that is capable of performing both 2D and 3D computations on any type of cylindrical finite difference grid. The model allows for an assessment of effects on mass transfer, gas holdup and bubble size of impeller type, impeller position, sparger position, aeration rate, etc.

The model predictions have been validated with experimental data regarding the local gas holdup, the local bubble size and several overall properties. In most cases the model predictions compare quite well with the experimental data. In the outflow of the impeller the model predictions and the experimental data tend to separate, due to the lack of good impeller models.

The spatial distributions of the important quantities (gas holdup, bubble size, mass transfer rate and turbulence) are all far from homogeneous. This seems to be a fundamental property of gassed stirred tanks. With all three impellers investigated, the highest mass transfer rates are found in the outflow of the impeller.

With the disc turbine about 31% of the total mass transfer rate takes place in the impeller outflow. With the axial flow impellers the spatial k_la distribution is a bit more homogeneous, leading to about 14% of the total mass transfer taking place in the impeller outflow of the pitched blade turbine.

In the investigated flow regimes, with the A315 and the PBT, the gas is dispersed from the trailing vortices shed from the impeller blades. Peaks in the holdup are found in these vortices.

Mass transfer performance may be improved by matching the positions of the extremes in the spatial distributions of the important quantities. The knowledge that full homogeneity will never be achieved should be used in the design and optimization process.

The approach followed in this paper, combining CFD with local measurements of important quantities, seems to be the only method to gain further insight in the processes occurring in a stirred tank.

Research in the area of gas-liquid mixing should concentrate on studying the local properties of the gas-liquid mixture. The current state of the art in CFD makes the development of reliable two-phase codes possible, which can act as both a design tool and a research tool.

NOMENCLATURE

a	long axis of ellipse, m
a_d	interfacial surface area, m^{-1}
A	surface area, m^2
b	short axis of ellipse, m
C	impeller to bottom clearance, m
C_∞	model constant
C_ω	model constant
C_*	model constant

C_λ	model constant
d	diameter m
d_s	sparger diameter, m
D	impeller swept diameter, m
$\mathbf{D}$	diffusion coefficient, m^2s^{-1}
Eo	Eötvös number
f	number of bubble collisions, $m^{-3}s^{-1}$
$\vec{F}_s$	slipforce vector, N
Fl_i	impeller pumping number ($=Q_i/ND^3$)
Fl_g	gas flow number ($= Q_g/ND^3$)
H	liquid level, m
J	particle/bubble flux, $m^{-2}s^{-1}$
k	turbulent kinetic energy per fluid mass, $m^{-2}s^2$
k_l	liquid side mass transfer coefficient, ms^{-1}
k_la	overall volumetric mass transfer coefficient, s^{-1}
K_w	friction coefficient
L_t	turbulent length scale, m
n	number of impeller blades
n_b	bubble number density, m^{-3}
$\dot{n}_{b,cb}$	change in bubble number density due to coalescence/breakup processes, $m^{-3}s^{-1}$
N	impeller rotational speed, s^{-1}
N_b	number of bubbles
P	power consumption, W
Po	impeller power number ($= P/\rho N^3D^5$)
Q_g	gassing rate, m^3s^{-1}
Q_l	liquid flow rate, m^3s^{-1}
r	radial coordinate (outwards positive), m
$\hat{r}$	unit vector in radial direction
S	impeller-sparger separation, m
S_g	gas source, m^3s^{-1}
Sc	Schmidt number ($\nu/\mathbf{D}$)
T	vessel diameter, m
u	axial velocity (downwards positive), ms^{-1}
$\bar{u}$	time-averaged velocity vector, ms^{-1}
$\tilde{u}$	fluctuating component of the velocity vector, ms^{-1}
$\bar{u}_s$	slip velocity vector, ms^{-1}
v	velocity, ms^{-1}
v	radial velocity (outwards positive), ms^{-1}
v_{sg}	superficial gas velocity ($4Q_g/(\pi T^2)$), ms^{-1}
V	volume, m
w	tangential velocity (with impeller positive), ms^{-1}
W	baffle width, m
X_c	net efficiency of the coalescence process
z	axial coordinate, 0 at liquid surface, m
$\hat{z}$	unit vector in axial direction

Greek Symbols

α	gas holdup
ε	turbulent energy dissipation rate, m^2s^{-3}
ε_{imp}	turbulent energy dissipation rate in impeller region, m^2s^{-3}
$\langle\varepsilon\rangle$	average energy dissipation rate (P/V_l), W/m^{-3}
ϕ	tangential coordinate (0° at baffle), °
η	dynamic viscosity, mPas
η_e	effective viscosity, Pas
λ_t	transport free path, m
ν	kinematic viscosity, m^2s^{-1}
ν_t	turbulent viscosity, m^2s^{-1}
ρ	density, kgm^{-3}
ω	effective coalescence/breakup frequency, s^{-1}

Subscripts

b	referring to bubble
d	referring to dispersion (volume)
g	gas, under gassed conditions or referring to gas phase
l	referring to liquid phase
u	ungassed conditions
i	in inlet gas
in	at gas input
net	referring to net particle flux
out	leaving the vessel
∞	referring to maximum stable bubble size

Abbreviations

ASM	Algebraic Stress Model
CFD	Computational Fluid Dynamics
DT	Disc Turbine (Rushton Turbine)
LRS	Large ring sparger
LDV	Laser Doppler Velocimetry
OTR	Oxygen Transfer Rate
PBT	Downwards pumping Pitched Blade Turbine, 6 blades at 45 blade angle
RMS	Root Mean Square
RSM	Reynolds Stress Model
SRS	Small ring sparger

REFERENCES

1. Harvey P. S., 1980, *PhD Thesis*, (University of Bath, United Kingdom).
2. Harvey P. S. and Greaves M., 1982a, Turbulent flow in an agitated vessel. Part 1: A predictive model, *Trans IChemE*, 60: 195–200.
3. Harvey P. S. and Greaves M., 1982b, Turbulent flow in an agitated vessel, Part 2: Numerical simulation and model predictions, *Trans IChemE*, 60: 201–210.
4. Issa R. I. and Gosman A. D., 1981, The computation of three-dimensional turbulent two-phase flow in mixed vessels, *Proc 2nd Int Conf Num Meth Lam Turb Flows, Venice, Italy.*
5. Looney M. K., Issa R. I., Gosman A. D. and Politis S., 1985, Modelling of the turbulent flow of solid/liquid suspensions in stirred vessels, *Fifth Int Conf on Mathematical Modelling, Berkeley, July 29–31.*
6. Pericleous K. A. and Patel M. K., 1987, The modelling of tangential and axial agitators in chemical reactors, *Physico Chemico Hydrodynamics* 8: 105–123.
7. Mann R., 1986, Gas-liquid stirred vessel mixers: Towards a unified theory based on networks-of-zones, *Chem. Eng. Res. Des*, 64, 23–34.
8. Mann R. and Hackett L. A., 1988, Fundamentals of gas-liquid mixing in a stirred vessel: An analysis using networks of zones, *Proc 6th Eur Conf Mixing, Pavia, Italy, May 24–26*, 321–328.
9. Trägärdh Ch., 1988, A hydrodynamic model for the simulation of an aerated agitated fed-batch fermenter, *Proc 2nd Int Conf Bioreactor Fluid Dynamics, Cambridge, UK, September 21–23*, 117–134.
10. Patterson G. K., 1991, Measurements and modelling of flow in gas sparged agitated vessels, *Proc 7th Eur Conf Mixing, Brugge, Belgium, September 18–20*, 209–215.
11. Bakker A. and Van den Akker H. E. A., 1994, Gas-liquid contacing with axial flow impellers, *Trans IChemE*, Part A, 72: 573–582.
12. Bakker A. and Van den Akker H. E. A., 1994, Single-phase flow in stirred reactors, *Trans IChemE*, Part A, 72: 583–593.
13. Bakker A. and Van den Akker H. E. A., 1991, A computational study on dispersing gas in a stirred reactor, *Proc 7th Eur Conf Mixing, Brugge, Belgium, September 18–20*, 199–207.
14. Rodi W., 1980, Turbulence models and their application in hydraulics—A state of the art review, (International Association for Hydraulic Research, Delft, The Netherlands).
15. Boysan F., 1984, Mathematical modelling of cyclone separators, *Selected Topics in Two-Phase Flow*, (Lecture Series no. 9, Trondheim), May 25.
16. Joshi J. B., Pandit A. B. and Sharma M. M., 1982, Mechanically agitated gas-liquid reactors. *Chem Eng Sci* 37: 813–844.
17. Pendlebury J. M., 1985, *Kinetic Theory*, (Adam Hilger Ltd, Bristol, England).
18. Morsi S. A. and Alexander A. J., 1972, An investigation of particle trajectories in two-phase flow systems, *J. Fluid Mechanics*, 2: 193–208.
19. Barnea E. and Mizrahi J., 1975, A generalized approach to the fluid dynamics of particulate systems, Part 2: Sedimentation and fluidisation of clouds of spherical liquid drops, *Can J Chem Eng*, 53: 461–469.
20. Hinze J. O., 1955, Fundamentals of the hydrodynamic mechanism of splitting in dispersion processes, *AIChE J*, 1: 289–295. *Proc 2nd Int Conf Num Meth Lam Turb Flows*, Venice, Italy.
21. Greaves M. and Barigou M., 1988, The internal structure of gas-liquid dispersions in a stirred reactor, Proc 6th Eur Conf Mixing, Pavia, Italy, May 22–24, 313–320.

22. Kawase Y. and Moo-Young M., 1990, Mathematical models for the design of bioreactors: Application of Kolmogoroff's theory of isotropic turbulence, *Chem Eng J*, 43: B19–B41.
23. Wellek R. M., Agrawal A. K. and Skelland A. H. P., 1966, Shape of liquid drops moving in liquid media, *AIChE J*, 12: 854–862.
24. Bakker A., 1992, Hydrodynamics of stirred gas-liquid dispersions, *PhD Thesis*, (Delft University of Technology, The Netherlands).
25. Frijlink J. J., 1987, Gassed suspension reactors, *PhD Thesis*, (Delft University of Technology, The Netherlands).
26. Bakker A. and Van den Akker H. E. A., 1990, Gas liquid contacting with the Lightnin A315 impeller; effects of flow pattern, *AIChE Annual Meeting, Chicago, November 11–16*, Session on Industrial Mixing and Scale-Up, Unpublished.

ADDRESS

Correspondence concerning this paper should be addressed to Dr A. Bakker, Chemineer Inc, 5870 Poe Avenue, Dayton, OH 45414, USA.

The manuscript was communicated via our International Editor for Continental Europe, Dr A. D. Barber. It was received 5 January 1992 and accepted for publication after revision 29 October 1993.